Master's thesis

NTNU
Norwegian University of Science and Technology
Faculty of Medicine and Health Sciences
Department of Circulation and Medical Imaging

Brita-Lill Pedersen Strømsmo

The Effect of Sampling Rate on Resting State Functional MRI

Master's thesis in medical imaging technology
Supervisor: Øystein Olsen
Co-supervisor: Torgil Riise Vangberg
May 2024

NTNU
Norwegian University of
Science and Technology

Brita-Lill Pedersen Strømsmo

The Effect of Sampling Rate on Resting State Functional MRI

Master's thesis in medical imaging technology
Supervisor: Øystein Olsen
Co-supervisor: Torgil Riise Vangberg
May 2024

Norwegian University of Science and Technology
Faculty of Medicine and Health Sciences
Department of Circulation and Medical Imaging

NTNU
Norwegian University of
Science and Technology

The Effect of Sampling Rate on Resting State Functional MRI

Abstrakt

Det har nylig blitt vist at variabiliteten i rs-fMRI (BOLD-variabilitet) kan være en sensitiv indikator på cerebral helse, hvor det er spekulert i om variabiliteten kan være relatert til arteriestivhet. En stor andel av variabiliteten i rs-fMRI signalet er fysiologisk variasjon som følge av hjerte og respirasjonsbevegelser. Denne høyfrekvente fysiologiske variabiliteten fører til foldingsfeil ved tradisjonelle rs-fMRI protokoller hvor repetisjonstider på 2 – 3 sekunder benyttes. Det er derfor ikke klart om variabiliteten i rs-fMRI kan beskrives tilstrekkelig ved tradisjonell temporal oppløsning (2 – 3 sekunder), eller om høyere temporal oppløsning, som unngår foldingsfeil av fysiologisk variabilitet, er nødvendig.

Målet ved denne studien var todelt: først en sammenligning mellom en BOLD-sekvens med lav temporal oppløsning (TR = 2500 ms) og en med høy temporal oppløsning (TR = 356 ms) for å vurdere om sekvensen med lav temporal oppløsning er tilstrekkelig for å beskrive variabiliteten, eller om høy temporal oppløsning, som unngår foldingsfeil av fysiologisk variabilitet, er nødvendig. Det andre målet var å teste om variabiliteten kan assosieres med fysiologiske målinger, spesielt arteriestivhet. Dette ble gjort ved å estimere pulsbølge-hastigheten i a. Carotis ved bruk av fasekontrast-angio.

En BOLD-sekvens med høy (TR = 356 ms) og en med lav (TR = 2500 ms) temporal oppløsning gjennomgikk en standard temporal filtrering (>0.01 Hz), og BOLD-variabiliteten ble beregnet i ufiltrerte datasett, standardfiltrerte datasett (>0.01 Hz) og lave frekvenser (VLF) (0.008 – 0.1 Hz) for begge fMRI-sekvensene. I tillegg ble BOLD-variabiliteten i respiratorisk (0.1 – 0.6 Hz) og hjertefrekvensområdet (>0.6 Hz) beregnet for BOLD-sekvensen med høy temporal oppløsning.

Resultatene viser at forskjellen mellom BOLD-sekvensen med høy temporal oppløsning og lav temporal oppløsning øker ved økende variabilitet. Det er derfor rimelig å anta at BOLD-sekvensen med lav temporal oppløsning ikke vil være tilstrekkelig til vurdering av høyfrekvent variabilitet. I tillegg er det fysiologiske bidraget til BOLD-variabiliteten bedre detektert ved

høy temporal oppløsning. Det ble imidlertid ikke funnet noen assosiasjon mellom BOLD-variabilitet og pulsbølge-hastighet som et mål på arteriestivhet.

Abstract

It has recently been shown that the variability in rs-fMRI (BOLD variability) may be a sensitive marker of cerebrovascular health, where it is speculated that the variability may be related to cerebrovascular compliance. However, a large part of the variability in the rs-fMRI signal is due to cardiorespiratory motion, which will be under sampled using traditional rs-fMRI protocols with repetition times of 2 – 3 seconds. It is, therefore, not clear whether the variability in the rs-fMRI signal will be adequately determined using traditional rs-fMRI scans or if it is necessary to scan with sufficiently high temporal resolution to avoid aliasing of the signal components related to cardiorespiratory motion.

The aim of the current study was twofold: First to compare the BOLD variability from a low temporal resolution rs-fMRI sequence (TR = 2500 ms) to that of a high temporal resolution rs-fMRI sequence (TR = 356 ms) in a sample of 28 healthy participants (22 – 50 years) to determine whether the low temporal resolution sequence can adequately describe BOLD variability or if it is necessary to scan with a temporal resolution that avoids aliasing of the cardiorespiratory components of the signal. Second, to test whether the variability can be associated with physiological measures, particularly with cerebrovascular compliance. This was done by estimating the pulse wave velocity (a proxy for arterial compliance) in the carotid artery using a phase contrast flow sequence.

A high (TR = 356 ms) and a low (TR = 2500 ms) temporal resolution BOLD sequence underwent temporal filtering (cutoff 0.01 Hz), and the BOLD variability was calculated in unfiltered datasets, standard filtered datasets (cutoff 0.01 Hz) and very low-frequency bands (0.008 — 0.1 Hz) for both fMRI sequences. Additionally, the BOLD variability in respiratory (0.1 — 0.6 Hz) and cardiac bands (> 0.6 Hz) were calculated for the high temporal resolution sequence.

The main findings were that the difference between the high and the low temporal resolution sequence increases as the variability increases. Therefore, it is reasonable to assume that the low temporal resolution sequence will be insufficient to detect higher variability accurately. In

addition, physiological contributions to BOLD variability are better detected in the high temporal resolution sequence. However, the study failed to find an association between BOLD variability and cerebrovascular compliance as measured by pulse wave velocity.

Introduction

Resting state functional magnetic resonance imaging (rs-fMRI) is a non-invasive method for assessment of low frequency changes in the brain during rest. However, there is a large variance in the rs-fMRI signal that is not caused by neuronal activity. As much as 20%-60% of the ‘’blood oxygen level dependent’’ (BOLD)-signal is due to physiological factors, where inflow effects and respiration are the primary contributors (Triantafyllou et al., 2005).

Blood flow in the cerebral microvasculature affects the BOLD-signal through pulsation, T1 inflow effects, changes in the intravascular oxygenation concentration and local modulation of the B0-field (Verstynen & Deshpande, 2011). The intravascular oxygen concentration may further lead to individual differences in the signal variance, where individuals with lower venous oxygen concentration have higher signal amplitude in the BOLD-signal and vice-versa (Lu et al., 2008). Body Mass Index (BMI), hemoglobin levels and blood pressure also affect the signal variance (Sjuls & Specht, 2022). Individual differences in blood pressure and BMI give small global differences in signal amplitude and duration of the BOLD-signal, respectively. In addition, the susceptibility changes related to respiratory motion give rise to distortions that vary across space and time (Liu, 2016). Respiration may also influence the signal indirectly through modulation of carbon dioxide (CO2) levels. CO2 is a vasodilator, so that blood flow effects can be time varying as a result of dynamic changes in CO2 concentration. The signal from these physiological factors will overlap in an unpredictable manner with the very low frequency (VLF) band that is usually of interest in fMRI studies if the TR is not sufficiently short (Huotari et al., 2019; Tong et al., 2019). If the TR is sufficiently short to sample the high-frequency cardiac signal, removing the signal via high-pass filtering is possible, but it requires a TR < 300 ms, which is challenging on most MR scanners.

It has also been found that the physiological component of the signal contains relevant clinical information. Patients with Alzheimer's disease have a significant increase in BOLD variability compared to healthy controls (Makedonov et al., 2016; Scarapicchia et al., 2018; Tuovinen et al., 2020). This increase in variance of the BOLD signal in elderly, Alzheimer patients and patients with cerebrovascular disease is assumed to be due to increased arterial stiffness in the cerebral microvasculature (Makedonov et al., 2013; Scheel et al., 2022). The observation that the physiological variability in Alzheimer patients is dominated by cardiac pulsatility, supports the idea that arterial stiffness is the main source of differences in BOLD variability (Tuovinen et al., 2020). These findings suggest that the physiological variability in the BOLD signal can be a useful indicator of cerebrovascular health.

Given a heart rate between 50-100 beats per minute (bpm) the frequency of the cardiac-related variability in the BOLD signal is in the range of 0.8 – 1.6 Hz (Tuovinen et al., 2020), it is necessary to scan with high temporal resolution to avoid aliasing of the cardiac related signal. This can be achieved by scanning with a low repetition time (TR). The sequence magnetic resonance encephalography (MREG) allows for TR down to 100 ms (Hennig et al., 2021). This technique is, however, hampered by complicated image reconstruction and low image quality. An alternative approach is to limit the number of slices acquired to achieve lower repetition times, but will result in images that only includes limited parts of the brain. A way around these obstacles could be the use of simultaneous multi slice (SMS) in combination with EPI-BOLD. This technique, which is sometimes called multiband fMRI, can drastically reduce the TR of acquisitions by reading the signal from several slices at once (Setsompop et al., 2012). This combination will allow for a low TR and inclusion of the entire brain in the imaging volume, and is also a more available option than MREG. The combination of SMS and EPI-BOLD to study the physiological variability in the BOLD-signal is to our knowledge not previously studied.

The primary goal of this study is to investigate if the BOLD-variability can be described adequately with a low temporal resolution BOLD sequence (TR = 2500 ms), or if a higher temporal resolution BOLD sequence that does not under sample physiological variance (mainly from cardiac and respiratory motion) is necessary. The secondary goal is to investigate how physiological differences impact the measured variability in a low and a high temporal

resolution BOLD-sequence. And lastly, to investigate whether the BOLD variability can be linked to arterial stiffness assessed by the pulse wave velocity (PWV).

It is hypothesized that:

1: High temporal resolution BOLD imaging will give more correct variability measurements compared to low temporal resolution BOLD imaging.

2: The association between BOLD variability and physiological measurements is more profound in high temporal resolution BOLD imaging.

3: Pulse wave velocity is associated with BOLD variability.

Materials and methods

Participants

A total of 28 participants between 22 and 50 years of age were included in this study. All participants were healthy volunteers with no relevant medical history. The study was approved by the regional ethics committee (REK #543087) and carried out in accordance with relevant guidelines and regulations at the University Hospital North Norway. All participants gave written informed consent before participating in the study.

Physiological measurements

The participant's blood pressure and pulse were measured on the left arm while seated immediately before the MRI was taken. The Body Mass Index (BMI) was calculated with the height and weight given by the participant. Table 1 gives key characteristics of the participants.

Table 1. Key characteristics of the participants. Values reported as median (interquartile range).

Characteristic	**Overall**, N = 28	**female**, N = 15	**male**, N = 13
Age (years)	33 (29, 38)	32 (29, 36)	33 (27, 39)
Diastolic blood pressure (mmHg)	82 (75, 90)	76 (74, 88)	88 (80, 92)
Systolic blood pressure (mmHg)	132 (119, 145)	122 (117, 132)	144 (131, 153)
Pulse rate (bpm*)	74 (67, 87)	72 (67, 82)	80 (71, 88)
Body mass index (kg/m²)	24.8 (22.1, 28.1)	22.6 (21.4, 25.8)	26.6 (24.1, 29.4)

*bpm = beats per minute

MRI acquisition

The MRI scanning was carried out on a Siemens Magnetom Skyra 3-Tesla scanner (Siemens AG, Germany) equipped with a 64-channel head/neck coil.

The high temporal resolution rs-fMRI sequence was optimized and tested on a healthy volunteer prior to the acquisition of data included in this study. Because multiple slices are acquired at once, images that are acquired with SMS are prone to slice leakage artifacts where signal from the simultaneous acquired slices spread across the respective slices (McNabb et al., 2020). The volunteer was given a finger tapping task with 20 seconds active and 20 seconds rest alternating for 5 minutes while the fMRI sequence was running. In the resulting activation map there were activation in the hand knob and no visual signs of slice leakage (see Appendix Figure 1).

The protocol included a quick survey of the brain, a sagittal T1 3D MPRAGE for anatomical reference (FOV=240mm, matrix=256, slice thickness=0.9 mm, AP phase encoding direction, TR/TE=2300 ms/2.32 ms, TI=900 ms, FA=8°, GRAPPA acceleration factor 2). A transverse 3D

Time of Flight (TOF) were obtained to plan the phase contrast image (FOV=200 mm, matrix=384, slice thickness=0.50 mm, RL phase encoding direction, TR/TE=21 ms/3.43 ms, FA=22°, GRAPPA acceleration factor 3).

To assess the BOLD-variance two T2* weighted rs-fMRI sequences were obtained. A high temporal resolution sequence (TR=356 ms), that avoids undersampling of the physiological components of the signal (FOV=225 mm, matrix=76, slice thickness=3 mm, RL phase encoding direction, TR/TE=356 ms/32 ms, FA=60°, GRAPPA acceleration factor 2 and Simultaneous Multi Slice (SMS) with acceleration factor 6, measurements=900), and a ‘‘standard’’ sequence with a commonly used temporal resolution of 2500 ms, which under samples the physiological components of the signal (FOV=225 mm, matrix=90, slice thickness=3 mm, AP phase encoding direction, TR/TE=2500 ms/30 ms, FA=90°, GRAPPA acceleration factor 2, measurements=120).

For measurement of blood flow velocity, a single slice sagittal phase contrast image (PCA) was taken over the left carotid artery (FOV=200 mm, matrix=224, slice thickness=6 mm, AP phase encoding direction, TR/TE=23.20 ms/3.35 ms, FA=10°, GRAPPA acceleration factor 2, and velocity encoding individually adjusted between 80 and 120 cm/s).

Table 2. Overview of the sequences and parameters used in the MRI protocol.

Scan	**3D T1 MPRAGE**	**3D TOF**	**rs-fMRI**	**rs-fMRI**	**PCA**
Sequence	GRE		SMS EPI BOLD	EPI BOLD	
Orientation*	sag	tra	tra	tra	sag
TR (ms)	2300	21	356	2500	23.2
TE (ms)	2.32	3.43	32	30	3.35
TI (ms)	900				
Phase direction	AP	RL	RL	AP	AP
FA (degrees)	8°	22°	60°	90°	10°
Matrix	256	384	76	90	224
Slice thickness (mm)	0.9	0.5	3	3	6
FOV (mm)	240	200	225	225	200
Grappa	2	3	2	2	2
SMS			6		
VENC (cm/s)					80-120
Volumes			900	120	

*) sag = sagittal slice orientation, tra = transversal slice orientation

Calculation of the pulse wave velocity

The pulse wave velocity (PWV) was calculated using the middle upstroke area (MUSA) method (Dogui et al., 2011; Pahlavian et al., 2021). The phase images were first converted to flow velocities using the following formula:

$$v = \frac{\varphi}{\pi} \cdot \text{venc} \qquad (1)$$

Where v is the velocity, φ is the phase (ranging from -π to π) and venc is the velocity sensitivity.

PWV was estimated from the flow measurements using software from our lab. First a program created a mask of the arteries by calculating the temporal standard deviation in the magnitude flow images (Figure 1A) and thresholding at two standard deviations above the mean (Figure 1B). The mask was manually edited using itk-SNAP v. 4.2.0 (http://www.itksnap.org/pmwiki/pmwiki.php) (Yushkevich et al., 2006) so it only contained a single arterial segment starting at the common carotid artery and ending in the internal carotid artery (Figure 1C).

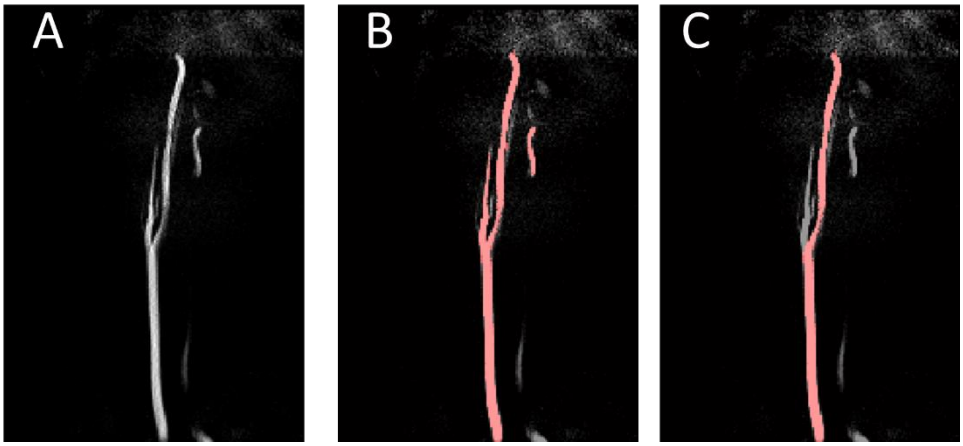

Figure 1. Masking of the carotid artery. The temporal standard deviation of the magnitude flow images was calculated to get a clear image of the arteries (**A**). A mask was created from the standard deviation image by thresholding it at > 2 (**B**). The mask was manually edited so that it only contained a single continuous segment of the common and internal carotid artery (**C**).

The edited mask was fed into another program that skeletonized the mask and sampled the velocity data from the points along the centerline. This data was used to calculate the PWV with

the MUSA method. The temporal signal profile along each point on the centerline (Figure 2A), starting with the most upstream point in the mask was extracted from the phase flow images and normalized to unity as illustrated in Figure 2B. The time difference between the bolus passage at a given point px and the mean signal profile (the transit time), where the mean were obtained by calculating the signal profile along all measured points along the centerline, were estimated as the aera of the trapezoid spanning the four points defined by where the signal intensity at point px have 20% and 80% intensity and similarly where the mean curve has 20% and 80% intensity divided by the height on the y-axis (Pahlavian et al., 2021). This simplifies to calculating the average of the time difference between the signal profile at px and the mean profile at 20% and 80% as illustrated in Figure 2C. The distance of each point along the artery was then plotted against the transit time and the PWV is the inverse slope of least-squares fit to the points (Figure 2D).

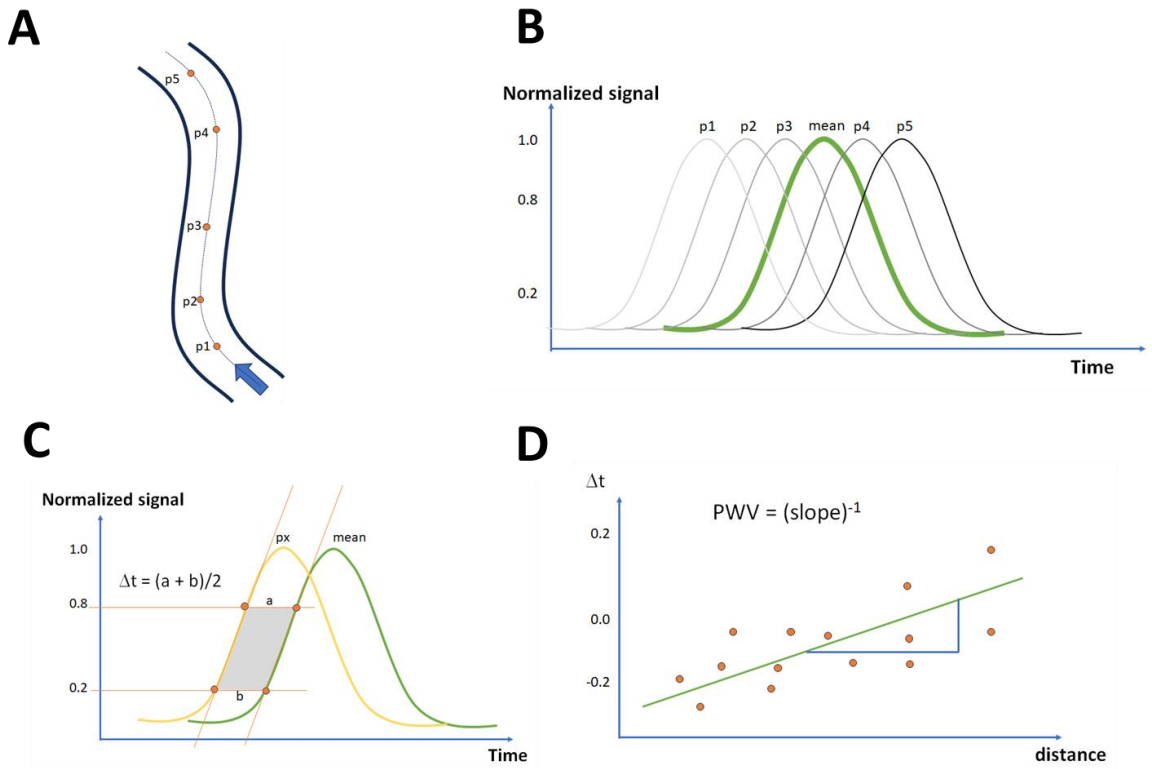

Figure 2. Illustration of how the pulse wave velocity were estimated by the MUSA method. The temporal signal evolution were sampled along points on the artery centerline (**A**). This was plotted in (**B**) where we see an idealized signal curve, illustrating the bolus passage, for each point. We see that upstream points reach a peak before downstream points. The green line represents the mean signal curve for all points. The time delay for the pulse wave at a given point px is estimated as the average of the delay at 20% and 80% signal intensity to the mean signal (**C**). The time lag is plotted against the distance for each point along the artery and the PWV is given as the slope of the least-squares fit (**D**).

BOLD variability maps

The BOLD variability maps for the low and high temporal resolution fMRI sequences were calculated similarly as in (Tuovinen et al., 2020). See Figure 3 and 4 for a flow chart of the processing pipelines. Briefly, the pipeline does the following.

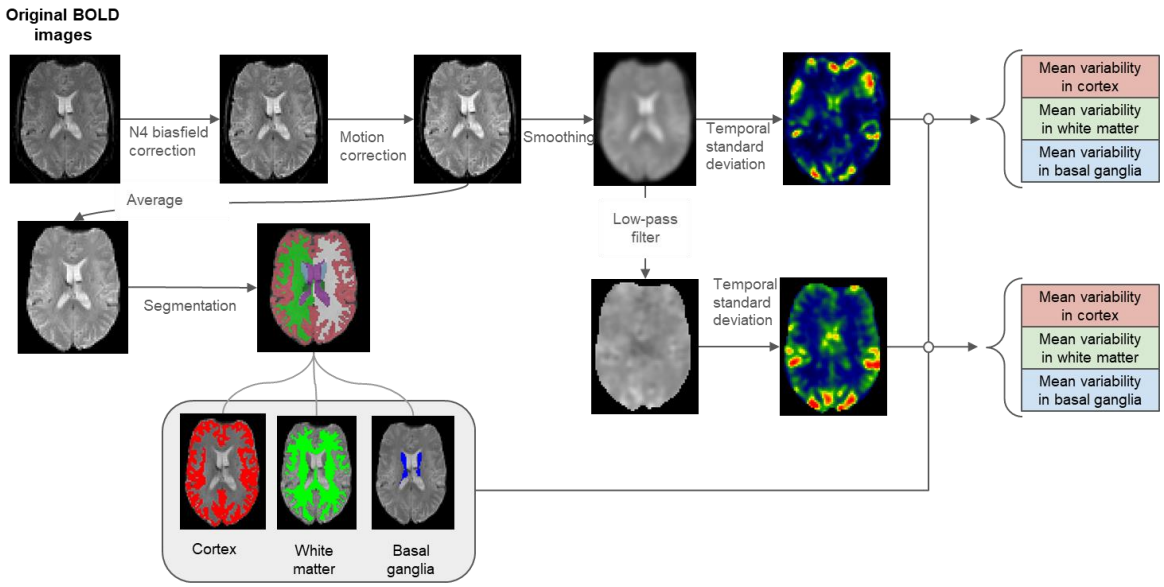

Figure 3. Image processing pipeline for the low temporal resolution fMRI data. The original BOLD images (upper left) were corrected for spatial intensity variations using a bias field correction algorithm, corrected for scan-to-scan motion and smoothed. An average image was calculated from the motion corrected images (middle left) and segmented into cortex and white matter, which was further used to construct a cortex, white matter and basal ganglia masks (bottom gray box). The temporal standard deviation was calculated from the smoothed images (top row), and low-pass filtered images (middle row). The average bold variability in cortex and white matter was calculated using the respective masks, from the temporal standard deviation of the unfiltered and low-pass filtered images (rightmost column).

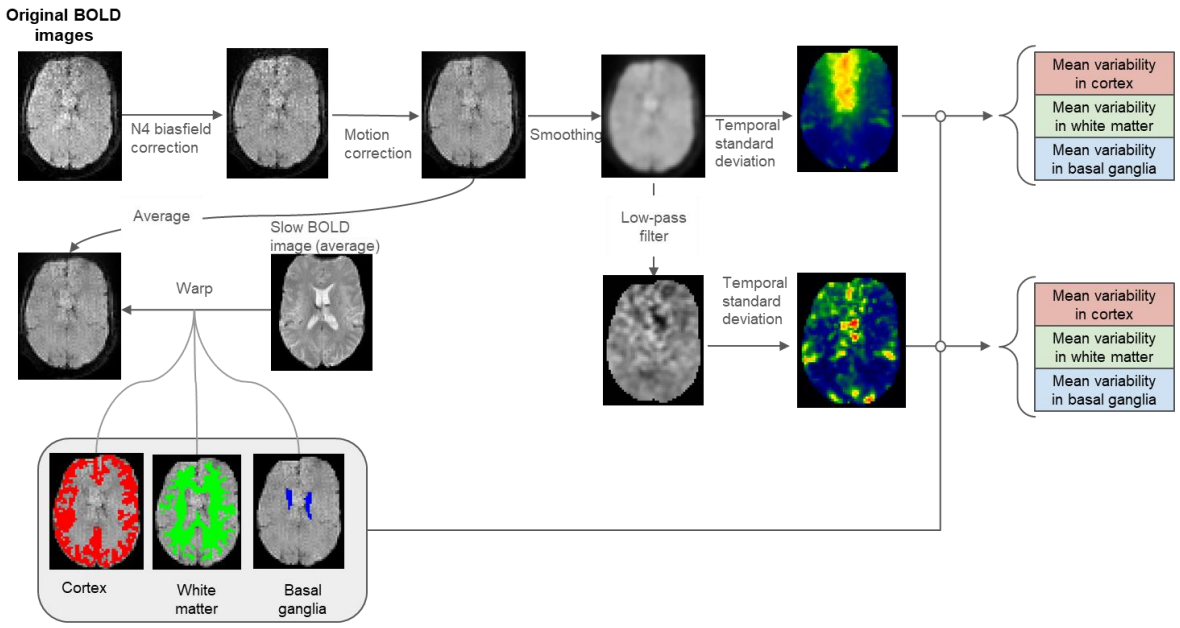

Figure 4. Image processing pipeline for the high temporal resolution fMRI data. The original BOLD images (upper left) were corrected for spatial intensity variations using a bias field correction algorithm, corrected for scan-to-scan motion and smoothed. An average image was calculated from the motion corrected images (middle left) and warped to the average BOLD image from the low temporal resolution fMRI sequence. The computed warp is used to transform the tissue masks from the low temporal resolution to the high temporal resolution fMRI image space. The temporal standard deviation was calculated from the smoothed images (top row), and low-pass filtered images (middle row). The average bold variability in cortex and white matter was calculated using the respective masks, from the temporal standard deviation of the unfiltered and low-pass filtered images (rightmost column).

Spatial variations in image intensities were corrected with the N4 bias correction algorithm in ANTS (version 2.4.3) (Tustison et al., 2010). Next, scan-to-scan motion in the fMRI series was corrected by registering the fMRI time series to the 1st volume using the antsMotionCorrection script in ANTS. Then, the fMRI images were smoothed with a 3 mm full-width-half maximum (FWHM) Gaussian kernel and temporal filtered (cutoff 0.01 Hz) using niimath (https://github.com/rordenlab/niimath, version 1.0). The BOLD variability maps were then calculated as the standard deviation of the BOLD time series. To probe whether the BOLD variability in specific frequency bands was differently associated with the physiological measurements, BOLD variability maps were calculated from the unfiltered datasets, standard filtered (cutoff 0.01 Hz), i.e., the filter commonly applied in rs-fMRI analyses, and very low-frequency bands (VLF), believed to primary reflect neuronal activity, (0.008 — 0.1 Hz) for both fMRI sequences. Additionally, the BOLD-variability in respiratory (0.1 — 0.6 Hz) and cardiac bands (> 0.6 Hz) were calculated for the high temporal resolution sequence. See Figure 5 and 6 for BOLD time series, and Figure 7 for illustration of BOLD variability maps.

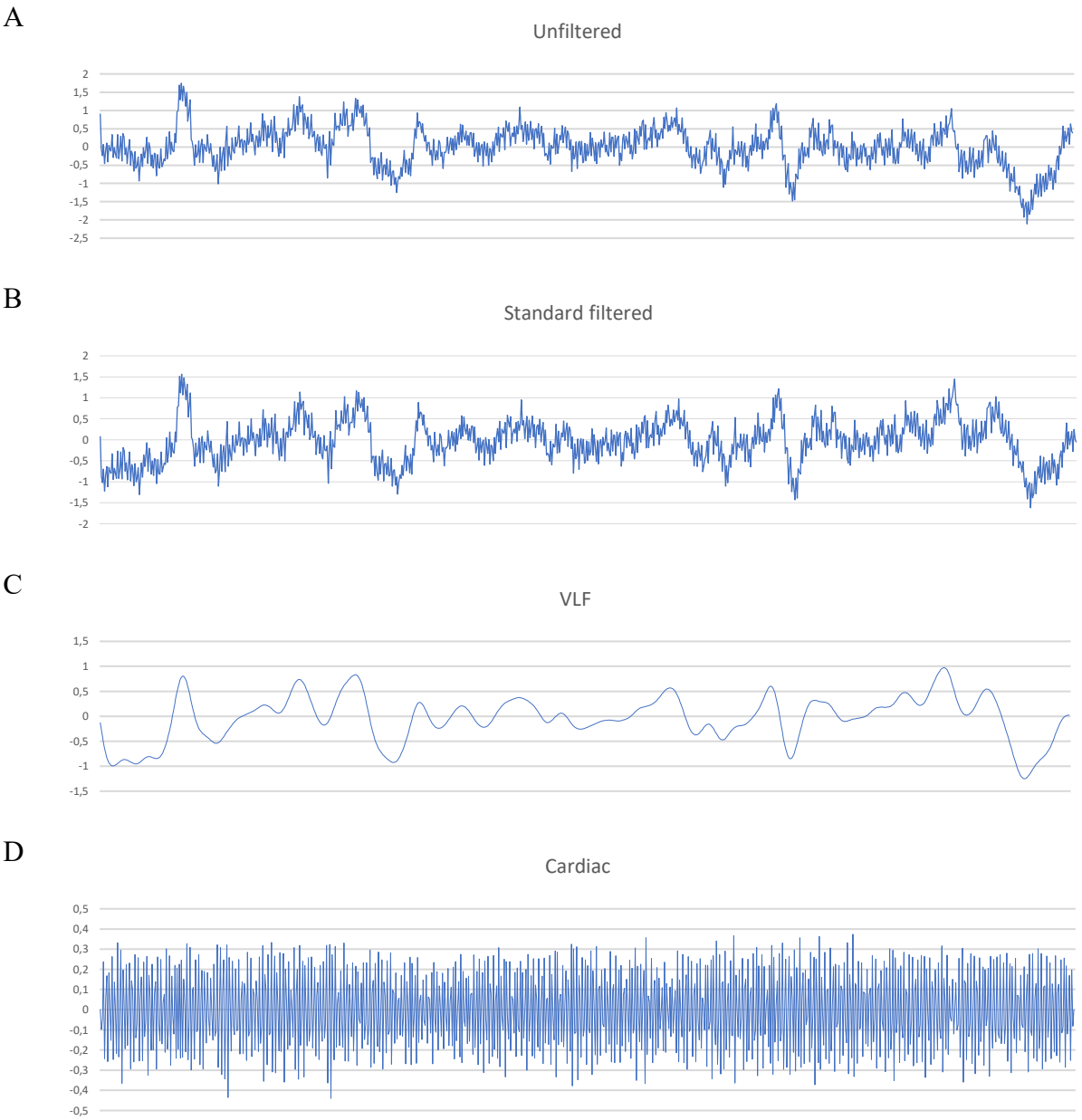

Figure 5. BOLD time series for the high temporal resolution BOLD sequence derived from cortex. **A:** unfiltered dataset, **B:** standard temporal filtered dataset (Cutoff 0.01 Hz), **C:** very low frequency (VLF) band (0.008 — 0.1 Hz) and **D:** cardiac band (>0.6 Hz)

Figure 6. BOLD time series for the low temporal resolution BOLD sequence derived from cortex. **A:** unfiltered dataset, **B:** standard temporal filtered dataset (Cutoff 0.01 Hz), and **C:** very low frequency (VLF) band (0.008 — 0.1 Hz).

The average BOLD-variability was extracted from cortical gray matter and cerebral white matter. The anatomical regions were derived by segmenting the average fMRI image from the low temporal resolution sequence after bias and motion correction using mri_synthseg version 2.0 (Billot et al., 2023). The segmentation from the low temporal resolution sequence was then warped to the high temporal resolution sequence using ANTS with a symmetric diffeomorphic mapping since direct segmentation of the high temporal resolution sequence with mri_synthseg was unreliable due to the lower contrast in these images.

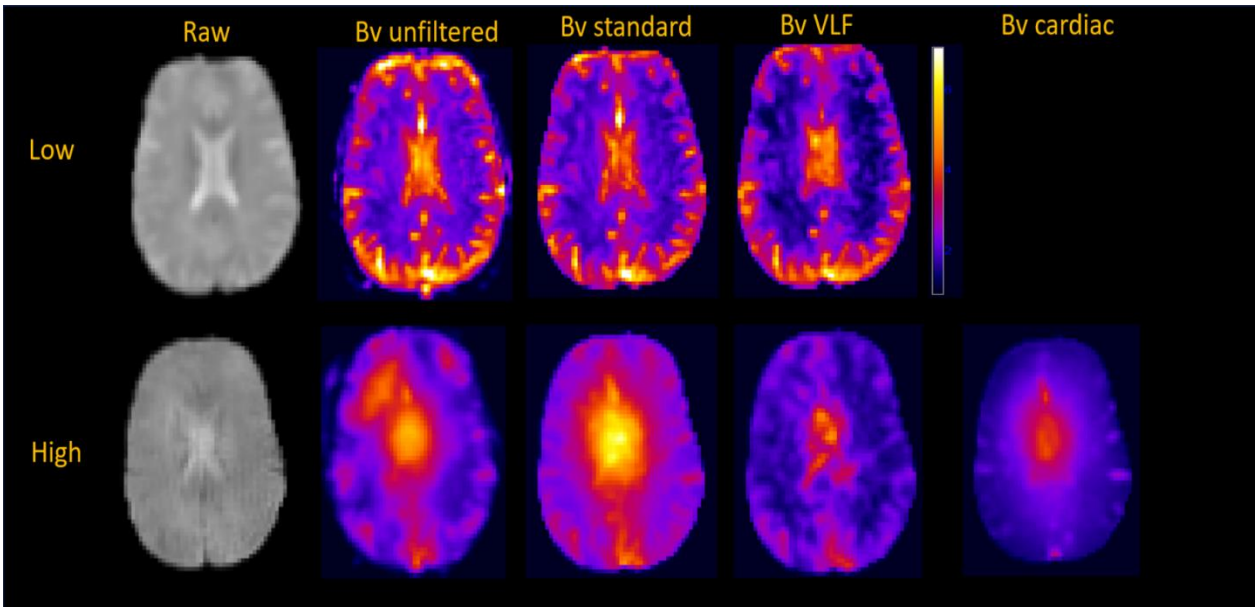

Figure 7. Illustration of BOLD variability (Bv) maps for the low (top row) and the high (bottom row) temporal resolution BOLD sequence. The left vertical column display raw images, followed by BOLD variability maps for the unfiltered images, standard filtered images (cutoff 0.01 Hz), very low frequency band images (0.008 — 0.1 Hz) and cardiac band images (>0.6 Hz) for the high temporal resolution sequence only.

Statistical analysis

BOLD variability has previously been associated with age (Makedonov et al., 2013) and several physiological measures: blood pressure, BMI (Sjuls & Specht, 2022), and heart rate (Shmueli et al., 2007). To understand the potential relationship between BOLD variability and the physiological measurements, Pearson correlation coefficients were calculated between the physiological variables (age, diastolic and systolic blood pressure, BMI, and pulse rate) and the BOLD variability maps (unfiltered, standard filtered, and VLF band for both the high and the low temporal resolution sequences, and a respiratory and cardiac filtered frequency band for the high temporal resolution sequence only). Significant correlations ($p < 0.05$) were assessed by a two-tailed Pearson correlation test. This analysis was carried out for both white matter and cortex. Subsequently, a linear regression analysis was conducted on the physiological variables, showing a significant correlation with the variability.

Bland-Altman plots were used to assess agreement between the BOLD variability maps obtained from the high (TR 356 ms) and low (TR 2500 ms) temporal resolution sequences. Additionally, linear regression analyses were separately conducted on the unfiltered, standard filtered and VLF band datasets, as well as between white matter and cortex, with the difference

between the two methods as the dependent variable and the mean between them as the independent variable.

To assess whether BOLD variability was associated with arterial stiffness as hypothesized (Tuovinen et al., 2020), a Pearson correlation were calculated between the BOLD variability maps and the estimated PWV from the Carotid artery.

All the statistical analyses were conducted in IBM SPSS (28.0.1.0 (142)), and the significance level was set to 0.05.

Results

Comparing high and low temporal resolution BOLD variability maps

Figure 8 shows the agreement between the unfiltered dataset (A), the standard filtered dataset (B) and the VLF band (C). There is agreement between the high and the low temporal resolution sequence in all the datasets with more than 95% of the difference being within the limits of agreement.

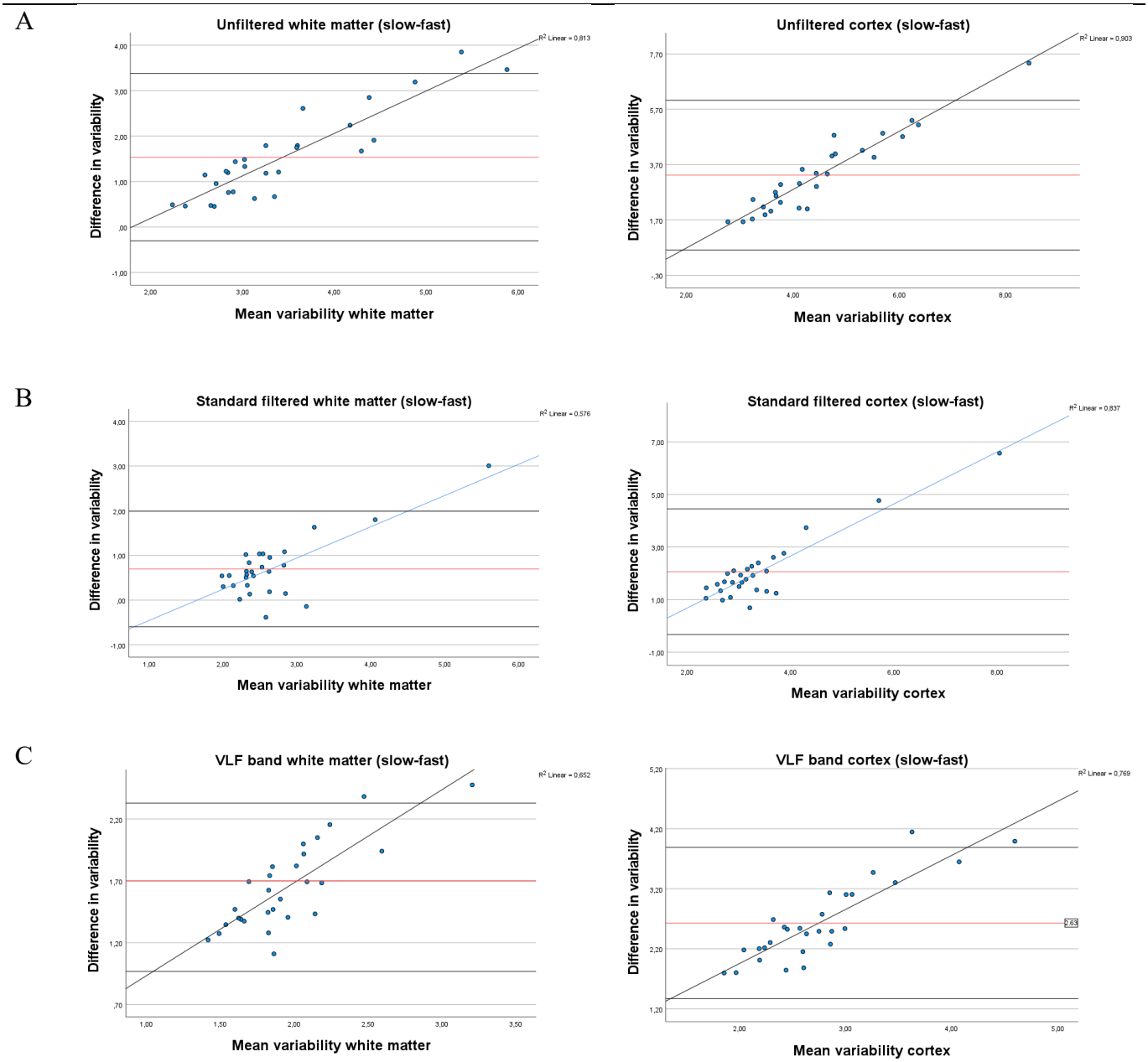

Figure 8. Bland-Altman plots of the agreement between the high and the low temporal resolution sequences. **A**: Unfiltered datasets. **B**: Standard filtered datasets and **C**: VLF band. A regression line is plotted for each dataset and for both white matter and cortex. The difference in variability between the two methods is calculated by subtracting the variability from the high temporal resolution sequence from the low temporal resolution sequence for the respective datasets. Mean variability is given by the mean between the two methods.

Table 3 shows the linear regression results for the difference between the high and the low temporal resolution sequence and the mean variability between the datasets. The linear relationship is positive and significant across all the frequency bands (unfiltered, standard filtered and VLF band).

Table 3. Regression table for the difference between high and low temporal resolution data.

Model	r	R^2	B	p value
Difference				
White matter				
Unfiltered	0.902	0.813	0.934	<0.001
Standard filtered	0.759	0.576	0.699	<0.001
VLF band	0.807	0.652	0.751	<0.001
Cortex				
Unfiltered	0.950	0.903	1.055	<0.001
Standard filtered	0.915	0.837	0.991	<0.001
VLF band	0.877	0.769	0.900	<0.001

Figure 9 show the mean variability for the low (A) and the high (B) temporal resolution sequence, for both white matter and cortex. The mean variability is shown for the unfiltered, standard filtered and VLF band for both sequences.

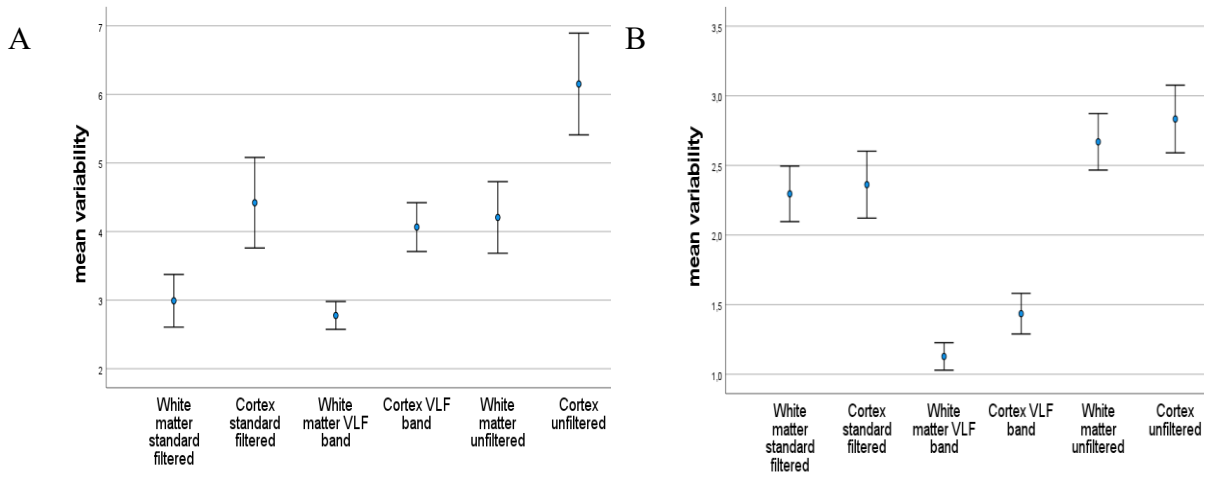

Figure 9. Mean variability with adjacent 95% confidence interval for the low (**A**) and the high (**B**) temporal resolution sequence. The mean variability is in general larger for cortex compared to white matter. This is the case for all the frequency bands included in the analysis (unfiltered, standard filtered and VLF band), and for both the high and the low temporal resolution sequence.

Physiological measurements and BOLD-variability

No significant relationship was observed between age, diastolic blood pressure, pulse rate, and BOLD variability (See Appendix Table 1). In contrast, a significant correlation was found between systolic blood pressure, BMI and variability across all frequency bands included in the analysis (Table 4 and 5).

BMI and BOLD variability

Table 4 shows the linear regression results for BMI and BOLD variability for the high and the low temporal resolution sequences. The table is divided into low temporal resolution (A) and high temporal resolution (B), and subdivided into white matter (A_1 and B_1) and cortex (A_2 and B_2).

The linear association is positive and significant across all frequency bands for both the high and the low temporal resolution sequence. The correlations range from r = 0.448 to r = 0.731 where the least correlated relationship is seen for the low temporal resolution sequence in the VLF band for cortex, and the highest correlation is seen for the high temporal resolution sequence in the standard filtered dataset for white matter.

Table 4. Estimates from the linear regression between BOLD variability measurements and BMI.

	Model	r	R^2	B	p value
A.	**Low temporal resolution and BMI**				
A.1	**White matter**				
	Unfiltered	0.620	0.384	0.194	<0.001
	Standard filtered	0.500	0.250	0.115	0.007
	VLF band	0.517	0.267	0.063	0.005
A.2	**Cortex**				
	Unfiltered	0.600	0.360	0.266	<0.001
	Standard filtered	0.471	0.222	0.186	0.011
	VLF band	0.448	0.201	0.096	0.017
B.	**High temporal resolution and BMI**				
B.1	**White matter**				
	Unfiltered	0.651	0.424	0.079	<0.001
	Standard filtered	0.731	0.535	0.087	<0.001
	VLF band	0.654	0.427	0.039	<0.001
	Cardiac band	0.720	0.518	0.032	<0.001
	Respiratory band	0.716	0.512	0.061	<0.001
B.2	**Cortex**				
	Unfiltered	0.587	0.344	0.085	0.001
	Standard filtered	0.664	0.441	0.096	<0.001
	VLF band	0.532	0.283	0.047	0.004
	Cardiac band	0.718	0.515	0.031	<0.001
	Respiratory band	0.678	0.460	0.068	<0.001

Systolic blood pressure and BOLD variability

Table 5 shows the linear regression results for systolic blood pressure and BOLD variability for the high and the low temporal resolution sequences. The table is divided into low temporal resolution (A) and high temporal resolution (B), and subdivided into white matter (A_1 and B_1) and cortex (A_2 and B_2).

Table 5. Estimates from the linear regression between BOLD variability measurements and systolic blood pressure (SBP).

	Model	r	R^2	B	p value
A.	**Low temporal resolution and SBP**				
A.1	**White matter**				
	Unfiltered	0.443	0.196	0.039	0.018
	Standard filtered	0.407	0.166	0.027	0.032
	VLF band	0.503	0.253	0.017	0.006
A.2	**Cortex**				
	Unfiltered	0.456	0.208	0.057	0.015
	Standard filtered	0.369	0.136	0.041	0.053
	VLF band	0.421	0.177	0.025	0.026
B.	**High temporal resolution and SBP**				
B.1	**White matter**				
	Unfiltered	0.609	0.370	0.021	<0.001
	Standard filtered	0.547	0.300	0.018	0.003
	VLF band	0.559	0.313	0.009	0.002
	Cardiac band	0.529	0.279	0.007	0.004
	Respiratory band	0.520	0.270	0.013	0.005
B.2	**Cortex**				
	Unfiltered	0.576	0.332	0.024	0.001
	Standard filtered	0.505	0.255	0.021	0.006
	VLF band	0.468	0.219	0.012	0.012
	Cardiac band	0.536	0.287	0.006	0.003
	Respiratory band	0.491	0.241	0.014	0.008

Pulse wave velocity

Table 6 shows the correlation results for pulse wave velocity and BOLD variability for the high and the low temporal resolution sequences. Due to noise in some of the PCA images, five of the pulse wave velocity results were discarded. No significant relationship was found between

the measured pulse wave velocity and BOLD variability. The closest association is seen in the unfiltered dataset for the low temporal resolution sequence with r = 0.18 and p = 0.41.

Table 6. Correlation table for pulse wave velocity and variability.

	Model	r	p value
A.	**Low temporal resolution and variability**		
A.1	**White matter**		
	Unfiltered	0.180	0.410
	Standard filtered	-0.106	0.632
	VLF band	0.033	0.881
A.2	**Cortex**		
	Unfiltered	0.133	0.545
	Standard filtered	-0.111	0.613
	VLF band	-0.021	0.926
B.	**High temporal resolution and variability**		
B.1	**White matter**		
	Unfiltered	0.071	0.749
	Standard filtered	0.000	0.999
	VLF band	-0.062	0.779
	Cardiac band	0.008	0.971
	Respiratory band	0.052	0.815
B.2	**Cortex**		
	Unfiltered	0.044	0.841
	Standard filtered	-0.037	0.865
	VLF band	-0.127	0.563
	Cardiac band	0.025	0.909
	Respiratory band	0.045	0.839

Discussion

The two main findings in this study were that it is necessary to use a temporal sampling rate that avoids aliasing the cardiac- and respiratory-induced fluctuations in the rs-fMRI signal to adequately measure the BOLD variability, and that systolic blood pressure and BMI significantly affect BOLD variability. The findings have implication for the understanding of which cardiovascular factors affect the BOLD variability. It is also likely that individual differences in BOLD variability may affect the strength in rs-fMRI networks, and as such this study also highlights the necessity of correcting for physiological noise in rs-fMRI studies.

Comparing high and low temporal resolution BOLD variability maps

The Bland-Altman plots in Figure 8 illustrate the agreement between the high and the low temporal resolution sequences with more than 95% of the difference being within the limits of agreement. The two methods are comparable for the lower variability, but it is evident that the disparity between the two methods increases as the variability increases. The relationship is linear, and as the variability increases, the low temporal resolution sequence's ability to describe rapidly fluctuating signal decreases. Previous research has shown a significant increase in variability in Alzheimer patients over a range of different temporal resolution imaging methods (ranging from TR=100 ms (MREG) to 3000 ms). However, the association between BOLD variability and Alzheimer's disease was strengthened with higher temporal resolutions (Tuovinen et al., 2020). The findings in this study are, therefore, consistent with previous findings in that there is a discrepancy between BOLD variability calculated from high and low temporal resolution data.

Table 3 indicates a strong positive relationship between the difference and the mean between the high and low temporal resolution scans. This relationship is seen for all the frequency bands included in this analysis (unfiltered, standard filtered and VLF band). The relationship is also seen for both white matter and cortex.

For white matter the unfiltered dataset exhibits a strong positive correlation ($r = 0.902$) and coefficient of determination value ($R^2 = 0.813$) between the difference and the mean variability. This indicates a high level of association between the variability and the difference between the methods, where 81.3% of the increasing difference can be explained by an increase in variability. Similarly, both the standard filtered and the VLF band datasets show a positive correlation ($r = 0.759$ and $r = 0.807$, respectively) between the difference and the mean variability. All the variability datasets show strong coefficient of determination values and significant regression coefficients ($p = <0.001$).

For cortex the correlation is slightly stronger for all the frequency bands (unfiltered, standard filtered and VLF band) compared to white matter ($r = 0.950$, $r = 0.915$ and $r = 0.877$, respectively). The coefficient of determination values is also stronger for cortex compared to

white matter, with the unfiltered dataset showing the strongest coefficient of determination (R^2 = 0.903). The regression coefficients are also larger compared to white matter. This could be explained by a larger variability in cortex in general (see Figure 9), and that the density of arteries and blood volume is larger in cortex than in white matter (Smirnov et al., 2021).

The standard filtered datasets are more centered around the mean compared to VLF band and unfiltered datasets (Figure 8B). This is expected as the high-pass filter (cutoff 0.01 Hz) removes portions of the aliased variance because of cardiac motion in the low temporal resolution sequence. This makes the high and the low temporal resolution sequences more comparable for lower variability. This is particularly seen in white matter, and is reflected in the regression analysis with the weakest coefficient of determination value (R^2 = 0.576).

In summary the linear relationship between the high and the low temporal resolution sequence is highly significant (p = <0.001) for both white matter and cortex, and for all the frequency bands examined in this analysis. These associations provide strong evidence that the high and low temporal resolution sequences do not give equal information regarding the BOLD variability as the variability increases. For potential clinical or research use of BOLD variability, where cases with high BOLD variability may be of primary interest, this suggests that high temporal resolution scans are necessary. The agreement in the lower spectrum of variability also suggests that the SMS EPI BOLD-sequence is of sufficient quality for the assessment of BOLD variability.

Physiological measurements and BOLD variability

There was no significant relationship between age, diastolic blood pressure, pulse rate, and the observed variability (See Appendix Table 1). These findings suggest that these physiological factors do not play a significant role in influencing the variability observed in the datasets. However, a correlation between age and BOLD variability has previously been found, where the variability tends to decrease in the older population compared to the younger population (Grady & Garrett, 2014). The age span included in this study (age 22 - 50) might not be sufficient to detect the same relationship. The association between variability and age also tend

to be spatially distinct, where the variability is increased in given areas of the brain, and decreased in others (Grady & Garrett, 2014; Tsvetanov et al., 2021). The segmentation in this study only included variability maps of cortex and white matter as a whole which will occlude potential spatial differences within these regions.

There is also an previous report of an association between diastolic blood pressure and global BOLD-signal where diastolic blood pressure is positively correlated with the strength of the BOLD signal (Sjuls & Specht, 2022). However, no significant association between diastolic blood pressure and BOLD variability was found in this study.

In contrast, a significant correlation was found between systolic blood pressure, BMI and BOLD variability across all frequency bands included in the analysis (Table 4 and 5). Notably, an exception was observed regarding the correlation between systolic blood pressure and the standard filtered dataset for cortex, where the relationship approached significance ($r = 0.369$, $p = 0.053$).

BMI and BOLD variability

For the low temporal resolution sequence there was a significant positive correlation between BMI and all the frequency bands included in this analysis (unfiltered, standard filtered and VLF band). Specifically, as BMI increases, variability tends to increase as well. This is the case for both white matter and cortex, whereas the strongest correlations were seen in white matter with correlations ranging from $r = 0.500$ (standard filtered) to $r = 0.620$ (unfiltered). In cortex, the correlations are slightly weaker compared to white matter, with correlations ranging from $r = 0.448$ (VLF band) to $r = 600$ (unfiltered). The strongest correlation is seen for the unfiltered dataset for both white matter and cortex. However, the linear relationship is significant for all the frequency bands and both anatomical regions.

Similarly to the low temporal resolution sequence, the high temporal resolution sequence has a significant positive correlation between BMI and variability across all frequency bands, including the cardiac and respiratory bands. Again, this is the case for both white matter and

cortex, whereas the strongest correlations were seen in white matter with correlations ranging from r = 0.651 (unfiltered) to r = 0.731 (standard filtered). The correlations in cortex are slightly weaker compared to white matter with correlations ranging from r = 0.532 (VLF band) to r = 0.718 (cardiac band). The linear relationship is significant for all the frequency bands and for both white matter and cortex.

It is not clear why BMI is associated with BOLD variability, but a higher BMI is believed to reduce cerebral blood volume (CBV) (Lemmens et al., 2006). The decreased CBV is thought to shorten the duration of the BOLD-signal (Sjuls & Specht, 2022). This mechanism could partially account for the observed association between BMI and BOLD variability. Additionally, BMI is positively correlated with systolic blood pressure (r = 0.511, p = 0.005), indicating that individuals with higher BMI tend to have elevated blood pressure levels. Given that systolic blood pressure is also linked to BOLD variability (Table 5), this relationship might further contribute to explaining the association between BMI and BOLD variability.

The results from the regression analysis between BMI and BOLD variability suggest that BMI is positively associated with the variability, regardless of the temporal resolution of the sequences and the brain regions examined. This indicates that higher BMI values are linked to increased variability in both white matter and cortex. However, the strength of the association varies slightly depending on the temporal resolution, frequency band and anatomical region. Overall, the high temporal resolution sequence correlates closer to BMI compared to the low temporal resolution sequence, and the strongest correlation is seen in the cardiac bands with r = 0.720 and r = 0.718 for white matter and cortex, respectively. The correlations in the respiratory bands follow the cardiac bands closely with r = 0.716 and r = 0.678 for white matter and cortex, respectively. Generally, the lowest correlations are seen for the VLF bands with the lowest observed correlation in cortex for the low temporal resolution sequence (r = 0.448). The correlations are also generally stronger in white matter compared to cortex.

Systolic blood pressure and BOLD variability

A similar trend is seen for the correlation between SBP and variability. For the low temporal resolution sequence, there is a significant but relatively weak positive correlation between SBP and variability across all frequency bands and anatomic regions. As mentioned, the only exception is a near significant regression coefficient between SBP and cortex in the standard filtered dataset for the low temporal resolution sequence ($p = 0.053$). For white matter the correlations range from $r = 0.407$ (standard filtered) to $r = 0.503$ (VLF band). Similar to the regression analysis between BMI and variability, the strongest correlation is seen for white matter. For cortex the correlations range from $r = 0.369$ (standard filtered) to $r = 0.503$ (unfiltered). The regression coefficients are all positive, indicating that an increase in SBP leads to an increase in variability.

For the high temporal resolution sequence, the correlation between SBP and variability is stronger than that of the low temporal resolution sequence. This is the case for both white matter and cortex, with white matter showing the strongest correlations (ranging from $r = 0.520$ to $r = 0.609$). Interestingly, the respiratory and the cardiac bands for white matter are the least correlated compared to the other frequency bands, with $r = 0.520$ and $r = 0.529$, respectively. The strongest correlation is seen in the unfiltered dataset. For cortex, the correlations are generally lower compared to white matter, with correlations ranging from $r = 0.468$ (VLF band) to $r = 0.576$ (unfiltered). The only exception is the correlations in the cardiac bands, where cortex has a slightly stronger correlation compared to white matter with $r = 0.536$ and $r = 0.529$, respectively. Similar to the low temporal resolution sequence, all the regression coefficients are positive.

BOLD-variance as a result of cardiac motion is reported to be dominant around major arteries and veins (Huotari et al., 2019), where higher blood pressure is believed to represent higher vascular resistance (Sjuls & Specht, 2022). The stronger correlation between systolic blood pressure and variability in white matter compared to gray matter could therefore be explained by the presence of larger vessels. Interestingly, the correlation is also stronger for white matter in the VLF-band. A possible explanation for this could be systemic low frequency oscillations (sLFO) (Tong et al., 2019), which is suggested to account for about 30% of the VLF-signal.

The sLFO's overlap the VLF signal one would expect as a result of neuronal activity, but since this in in white matter the sources are believed to be related to blood flow and possible fluctuations in CO2 concentrations.

Pulse wave velocity

No significant relationship was found between pulse wave velocity and BOLD variability (Table 6). The correlation coefficients vary from negative to positive values between the frequency bands and are r = 0.000 for the standard filtered dataset in white matter from the high temporal resolution sequence (Table 6, section B1). This suggests that variations in pulse wave velocity do not significantly impact the observed variability. However, a previous study observed a negative association between aortic pulse wave velocity and BOLD variance in spatially distinct gray matter areas (Hussein et al., 2020). In the same study, there was no significant association when the mean variability across all cortex and white matter was analyzed. In addition, Hussein et al (2020) found no significant relationship between PWV and variability in the younger population studied.

In Alzheimer patients the variability is increased compared to healthy controls (Tuovinen et al., 2020). The variability in the cardiac and the respiratory frequency bands is spatially distinct and are the main contributor to variability in this patient group. These changes are believed to be caused by arterial stiffness. However, the results of this study are unable to find evidence of this relationship. Overall, these findings underscore the complex interplay between vascular physiology and BOLD variability characteristics.

Limitations

The spatial resolution of the fMRI sequences is quite poor compared to anatomical imaging. Hence, it is therefore reasonable to assume that the variability maps are susceptible to partial volume effects. This is likely of most importance in cortex, where the anatomical structure is less spatially distinct.

There was no significant correlation between blood flow velocity and variability. This might be due to low SNR in the phase contrast images. Also, the TR was likely set too high for precise measurements depending on the heart rate. In addition, the acquisition was only a single slice of 6 mm which made it difficult to include both a. Carotis and a. Carotis interna equally for all the participants. This could have biased the measured pulse wave velocity between subjects. More reliable results could have been achieved with a 4D flow sequence, but this option was discarded due to the long acquisition time (~10 min) and complex post-processing.

Voxel-wise analysis might have been a better approach regarding correlation analysis between physiological measurements and BOLD variability. Particularly for analyzing the relationship between pulse wave velocity and variability, since previous studies have implied a spatially distinct relationship between these factors (Hussein et al., 2020; Tuovinen et al., 2020). However, voxel-wise analysis requires complex spatial normalization and statistical analysis of the data. In addition to this, the age span included in this study might not have been large enough to find any association between age and/or pulse wave velocity.

Conclusion

The results of this study imply that there is an agreement between the high and the low temporal resolution sequence for lower variability. However, the difference between the two methods increases as the variability increases. It is therefore reasonable to assume that the low temporal resolution sequence will be insufficient to detect higher variability accurately.

BMI is positively associated with variability across all frequency bands included in this analysis. However, the association is slightly stronger in the high temporal resolution sequence compared to the low temporal resolution sequence. As expected, the associations were also generally stronger in the cardiac and respiratory frequency bands. In addition, the association was stronger in white matter compared to cortex.

Similarly, SBP is positively associated with variability, with higher SBP being linked to increased variability. This association is also more pronounced in the high temporal resolution sequence compared to the low temporal resolution sequence, and the associations are generally stronger in white matter compared to cortex. These observations confirm the hypothesis that physiological contributions to BOLD variability are better detected in the high temporal resolution sequence.

No evidence of any association between pulse wave velocity and mean variability across cortex and white matter in relatively young and healthy adults could be found. Therefore, the findings do not lend support to our hypothesis that BOLD variability is associated with arterial stiffness.

In summary, the study shows that BOLD variability is sensitive to BMI and systolic blood pressure, providing further evidence that BOLD variability is sensitive to cerebrovascular health. However, as the potential mechanisms behind these associations are unclear, more research into the complex relationship between vascular physiology and pathology and BOLD variability is needed.

References

Billot, B., Greve, D. N., Puonti, O., Thielscher, A., Van Leemput, K., Fischl, B., Dalca, A. V., & Iglesias, J. E. (2023). SynthSeg: Segmentation of brain MRI scans of any contrast and resolution without retraining. *Medical Image Analysis*, *86*, 102789. https://doi.org/10.1016/j.media.2023.102789

Dogui, A., Redheuil, A., Lefort, M., DeCesare, A., Kachenoura, N., Herment, A., & Mousseaux, E. (2011). Measurement of aortic arch pulse wave velocity in cardiovascular MR: Comparison of transit time estimators and description of a new approach. *Journal of Magnetic Resonance Imaging*, *33*(6), 1321–1329. https://doi.org/10.1002/jmri.22570

Grady, C. L., & Garrett, D. D. (2014). Understanding variability in the BOLD signal and why it matters for aging. *Brain Imaging and Behavior*, *8*(2), 274–283. https://doi.org/10.1007/s11682-013-9253-0

Hennig, J., Kiviniemi, V., Riemenschneider, B., Barghoorn, A., Akin, B., Wang, F., & LeVan, P. (2021). 15 Years MR-encephalography. *Magma (New York, N.Y.)*, *34*(1), 85–108. https://doi.org/10.1007/s10334-020-00891-z

Huotari, N., Raitamaa, L., Helakari, H., Kananen, J., Raatikainen, V., Rasila, A., Tuovinen, T., Kantola, J., Borchardt, V., Kiviniemi, V. J., & Korhonen, V. O. (2019). Sampling Rate Effects on Resting State fMRI Metrics. *Frontiers in Neuroscience*, *13*, 279. https://doi.org/10.3389/fnins.2019.00279

Hussein, A., Matthews, J. L., Syme, C., Macgowan, C., MacIntosh, B. J., Shirzadi, Z., Pausova, Z., Paus, T., & Chen, J. J. (2020). The association between resting-state functional magnetic resonance imaging and aortic pulse-wave velocity in healthy adults. *Human Brain Mapping*, *41*(8), 2121–2135. https://doi.org/10.1002/hbm.24934

Lemmens, H. J. M., Bernstein, D. P., & Brodsky, J. B. (2006). Estimating blood volume in obese and morbidly obese patients. *Obesity Surgery*, *16*(6), 773–776. https://doi.org/10.1381/096089206777346673

Liu, T. T. (2016). Noise contributions to the fMRI signal: An overview. *NeuroImage*, *143*, 141–151. https://doi.org/10.1016/j.neuroimage.2016.09.008

Lu, H., Zhao, C., Ge, Y., & Lewis-Amezcua, K. (2008). Baseline blood oxygenation modulates response amplitude: Physiologic basis for intersubject variations in functional MRI signals. *Magnetic Resonance in Medicine*, *60*(2), 364–372. https://doi.org/10.1002/mrm.21686

Makedonov, I., Black, S. E., & Macintosh, B. J. (2013). BOLD fMRI in the white matter as a marker of aging and small vessel disease. *PloS One*, *8*(7), e67652. https://doi.org/10.1371/journal.pone.0067652

Makedonov, I., Chen, J. J., Masellis, M., & MacIntosh, B. J. (2016). Physiological fluctuations in white matter are increased in Alzheimer's disease and correlate with neuroimaging and cognitive biomarkers. *Neurobiology of Aging*, *37*, 12–18. https://doi.org/10.1016/j.neurobiolaging.2015.09.010

McNabb, C. B., Lindner, M., Shen, S., Burgess, L. G., Murayama, K., & Johnstone, T. (2020). Inter-slice leakage and intra-slice aliasing in simultaneous multi-slice echo-planar images. *Brain Structure and Function*, *225*(3), 1153–1158. https://doi.org/10.1007/s00429-020-02053-2

Pahlavian, S. H., Cen, S. Y., Bi, X., Wang, D. J. J., Chui, H. C., & Yan, L. (2021). Assessment of carotid stiffness by measuring carotid pulse wave velocity using a single-slice oblique-sagittal phase-contrast MRI. *Magnetic Resonance in Medicine*, *86*(1), 442–455. https://doi.org/10.1002/mrm.28677

Scarapicchia, V., Mazerolle, E. L., Fisk, J. D., Ritchie, L. J., & Gawryluk, J. R. (2018). Resting State BOLD Variability in Alzheimer's Disease: A Marker of Cognitive Decline or Cerebrovascular Status? *Frontiers in Aging Neuroscience*, *10*, 39. https://doi.org/10.3389/fnagi.2018.00039

Scheel, N., Tarumi, T., Tomoto, T., Cullum, C. M., Zhang, R., & Zhu, D. C. (2022). Resting-state functional MRI signal fluctuation amplitudes are correlated with brain amyloid-β deposition in patients with mild cognitive impairment. *Journal of Cerebral Blood Flow and Metabolism :*

Official Journal of the International Society of Cerebral Blood Flow and Metabolism, *42*(5), 876–890. https://doi.org/10.1177/0271678X211064846

Setsompop, K., Gagoski, B. A., Polimeni, J. R., Witzel, T., Wedeen, V. J., & Wald, L. L. (2012). Blipped-controlled aliasing in parallel imaging for simultaneous multislice echo planar imaging with reduced g-factor penalty. *Magnetic Resonance in Medicine*, *67*(5), 1210–1224. https://doi.org/10.1002/mrm.23097

Shmueli, K., van Gelderen, P., de Zwart, J. A., Horovitz, S. G., Fukunaga, M., Jansma, J. M., & Duyn, J. H. (2007). Low-frequency fluctuations in the cardiac rate as a source of variance in the resting-state fMRI BOLD signal. *NeuroImage*, *38*(2), 306–320. https://doi.org/10.1016/j.neuroimage.2007.07.037

Sjuls, G. S., & Specht, K. (2022). Variability in Resting-State Functional Magnetic Resonance Imaging: The Effect of Body Mass, Blood Pressure, Hematocrit, and Glycated Hemoglobin on Hemodynamic and Neuronal Parameters. *Brain Connectivity*. https://doi.org/10.1089/brain.2021.0125

Smirnov, M., Destrieux, C., & Maldonado, I. L. (2021). Cerebral white matter vasculature: Still uncharted? *Brain : A Journal of Neurology*, *144*(12), 3561–3575. https://doi.org/10.1093/brain/awab273

Tong, Y., Hocke, L. M., & Frederick, B. B. (2019). Low Frequency Systemic Hemodynamic “Noise” in Resting State BOLD fMRI: Characteristics, Causes, Implications, Mitigation Strategies, and Applications. *Frontiers in Neuroscience*, *13*, 787. https://doi.org/10.3389/fnins.2019.00787

Triantafyllou, C., Hoge, R. D., Krueger, G., Wiggins, C. J., Potthast, A., Wiggins, G. C., & Wald, L. L. (2005). Comparison of physiological noise at 1.5 T, 3 T and 7 T and optimization of fMRI acquisition parameters. *NeuroImage*, *26*(1), 243–250. https://doi.org/10.1016/j.neuroimage.2005.01.007

Tsvetanov, K. A., Henson, R. N. A., Jones, P. S., Mutsaerts, H., Fuhrmann, D., Tyler, L. K., & Rowe, J. B. (2021). The effects of age on resting-state BOLD signal variability is explained by

cardiovascular and cerebrovascular factors. *Psychophysiology*, *58*(7), e13714. https://doi.org/10.1111/psyp.13714

Tuovinen, T., Kananen, J., Rajna, Z., Lieslehto, J., Korhonen, V., Rytty, R., Mattila, H., Huotari, N., Raitamaa, L., Helakari, H., Abou Elseoud, A., Krüger, J., Levan, P., Tervonen, O., Hennig, J., Remes, A., Nedergaard, M., & Kiviniemi, V. (2020). The variability of functional MRI brain signal increases in Alzheimer's disease at cardiorespiratory frequencies. *Scientific Reports*, *10*. https://doi.org/10.1038/s41598-020-77984-1

Tustison, N. J., Avants, B. B., Cook, P. A., Yuanjie Zheng, Egan, A., Yushkevich, P. A., & Gee, J. C. (2010). N4ITK: Improved N3 Bias Correction. *IEEE Transactions on Medical Imaging*, *29*(6), 1310–1320. https://doi.org/10.1109/TMI.2010.2046908

Verstynen, T. D., & Deshpande, V. (2011). Using pulse oximetry to account for high and low frequency physiological artifacts in the BOLD signal. *NeuroImage*, *55*(4), 1633–1644. https://doi.org/10.1016/j.neuroimage.2010.11.090

Yushkevich, P. A., Piven, J., Hazlett, H. C., Smith, R. G., Ho, S., Gee, J. C., & Gerig, G. (2006). User-guided 3D active contour segmentation of anatomical structures: Significantly improved efficiency and reliability. *NeuroImage*, *31*(3), 1116–1128. https://doi.org/10.1016/j.neuroimage.2006.01.015

Appendix

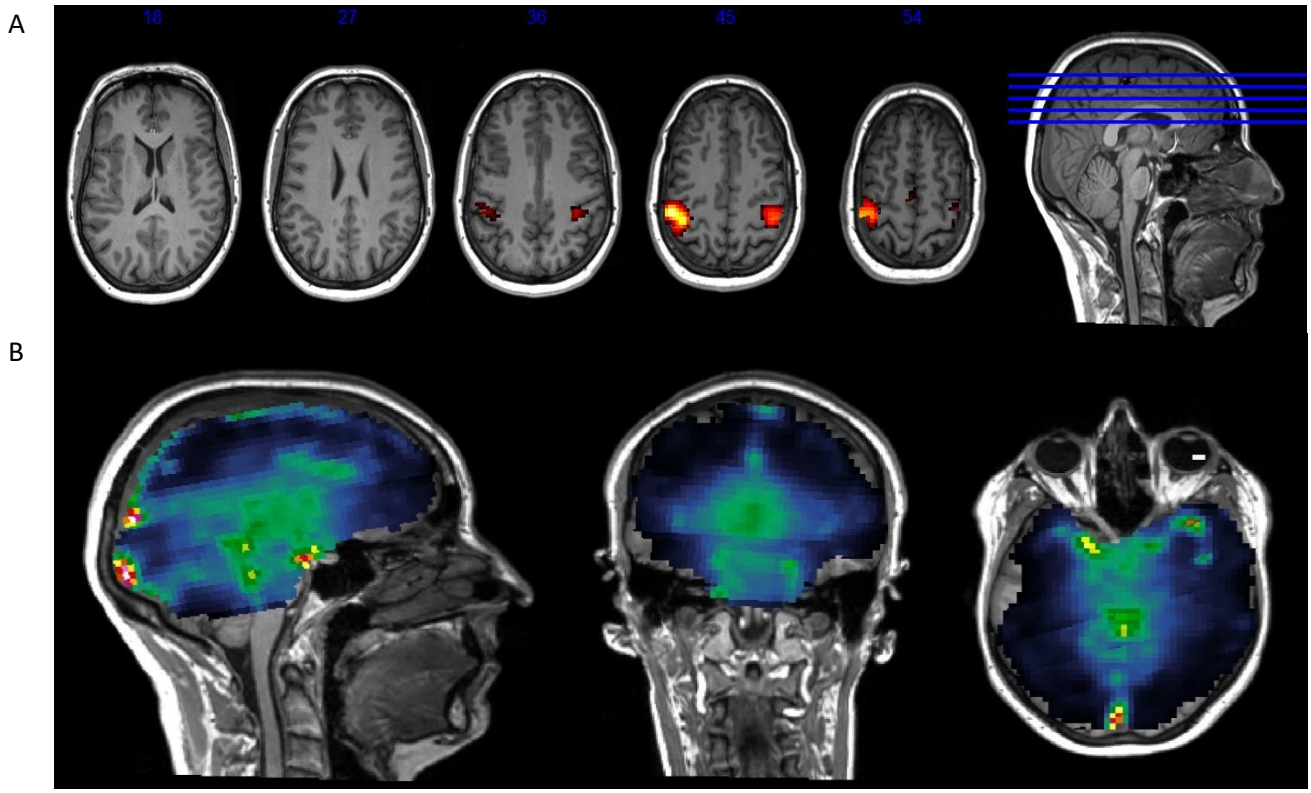

Figure 1. Quality test for the high temporal resolution fMRI sequence acquired prior to the data included in this study. The fMRI data was modelled with a block design with 20 seconds of rest and 20 seconds of active finger-tapping. Motion correction and a smoothing filter (8 mm FWHM kernel) were applied, and the analysis was done with SPM12 (https://www.fil.ion.ucl.ac.uk/spm/software/spm12/). **A:** Results from the finger-tapping paradigm with activation in the hand knob and no visual signs of slice leakage (false discovery rate corrected $p < 0.05$). **B:** Residual map generated from the finger-tapping paradigm, with noise around the ventricles and large vessels. There are no visual signs of systematic noise or artifacts in the brain parenchyma.

Table 1. Correlation table for physiological measurements and variability.

		pulse rate	DBP*	age
A.	**Low temporal resolution**			
A.1	**White matter**			
	Unfiltered	r=0.361 (p=0.059)	r=0.257 (p=0.187)	r=-0.025 (p=0.901)
	Standard filtered	r=0.049 (p=0.803	r=0.068 (p=0.731)	r=0.077 (p=0.699)
	VLF band	r=0.159 (p=0.419)	r=0.268 (p=0.168)	r=0.139 (p=0.481)
A.2	**Cortex**			
	Unfiltered	r=0.304 (p=0.115)	r=0.208 (p=0.287)	r=-0.037 (p=0.852)
	Standard filtered	r=0.008 (p=0.966)	r=0.032 (p=0.872)	r=0.054 (p=0.785)
	VLF band	r=0.045 (p=0.819)	r=0.183 (p=0.352)	r=0.092 (p=0.643)
B.	**High temporal resolution**			
B.1	**White matter**			
	Unfiltered	r=0.341 (p=0.076)	r=0.369 (p=0.053)	r=0.037 (p=0.851)
	Standard filtered	r=0.134 (p=0.498)	r=0.264 (p=0.175)	r=0.030 (p=0.878)
	VLF band	r=0.117 (p=0.553)	r=0.328 (p=0.088)	r=0.128 (p=0.518)
	Cardiac band	r=0.196 (p=0.318)	r=0.337 (p=0.079)	r=-0.049 (p=0.806)
	Respiratory band	r=0.136 (p=0.489)	r=0.202 (p=0.302)	r=0.023 (p=0.908)
B.2	**Cortex**			
	Unfiltered	r=0.326 (p=0.090)	r=0.340 (p=0.077)	r=0.071 (p=0.721)
	Standard filtered	r=0.078 (p=0.694)	r=0.215 (p=0.273)	r=0.067 (p=0.736)
	VLF band	r=0.039 (p=0.842)	r=0.272 (p=0.162)	r=0.124 (p=0.528)
	Cardiac band	r=0.171 (p=0.383)	r=0.302 (p=0.119)	r=-0.001 (p=0.997)
	Respiratory band	r=0.117 (p=0.553)	r=0.157 (p=0.424)	r=0.038 (p=0.848)

*) DPB= diastolic blood pressure.

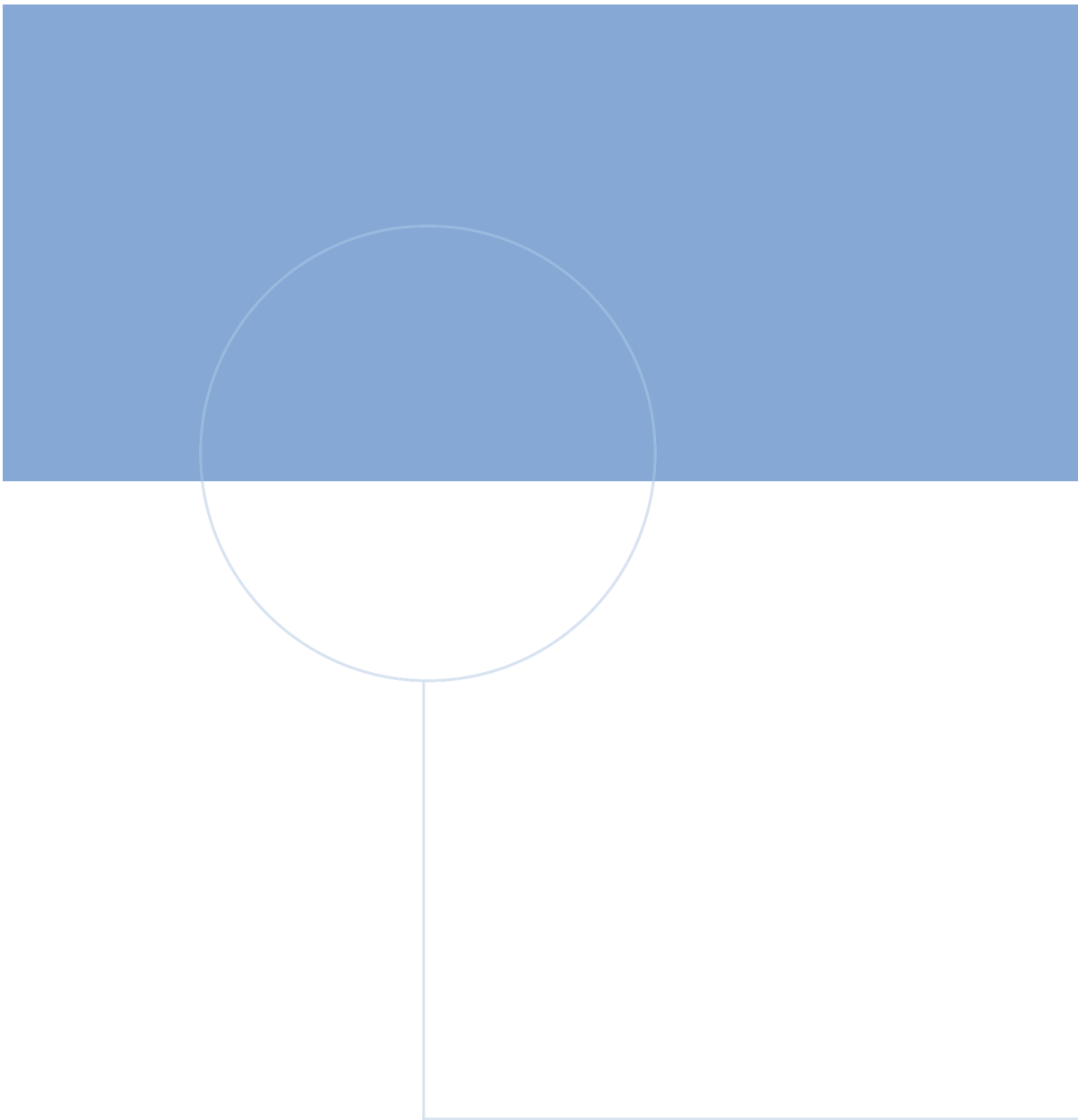

NTNU

Norwegian University of
Science and Technology